UDC 5 54 544.654.2

STUDY OF THE PROCESS OF ELECTROREDUCTION OF ANTIMONY IONS FROM AN ACIDIC ELECTROLYTE

N.A. Aliyeva Mammadova[1*], S.F. Jafarova[1], S.P. Javadova[1], Sh.A. Ibrahimova[2], A.A. Aliyev[3], S.D. Dadashova[1], M.F. Nabiyeva[1], M.T.Abbasov[1], H.Ch. Aliyeva[4], D.B. Tagiyev[1]

[1]"Institute of Chemistry" Public Legal Entity, MSE of the Azerbaijan Republic, AZ 1143, ave. H. Javid 113, Baku, Azerbaijan
[2]Azerbaycan Sport Academy, F.Kh. Khoysky Ave. 98, Baku, Azerbaijan
[3]Institute of Physics of MSE Azerbaijan Republic, H. Javid Ave., 131, Baku, Azerbaijan
[4]Institute of Petrochemical Processes named after acad. Y.H. Mammadaliyev Ministry of Science and Education of the Azerbaijan Republic, Az 1025, Baku, Xodjaly Ave., 30

*vuska_80@mail.ru

Received 26.02.2026
Reviewed 28.03.2026
Accepted 30.04.2026

The process of electroreduction of antimony ions from an acidic electrolyte was studied. The potential range of electroreduction of antimony ions at various electrodes was determined by plotting cyclic polarization curves. The influence of several factors on the electroreduction process of antimony was also studied. It was found that increasing the temperature increases the rate of electroreduction of antimony ions. Moreover, polarization curves were plotted using a rotating platinum disk electrode. The data obtained, namely the linear dependence of i_p on the electrode rotation speed (ω), confirm that the process of electroreduction of antimony ions is accompanied by diffusion kinetics. The dependence of current density on the electrode rotation speed at different potentials also confirms this result.

Keywords: *antimony ions, polarization, electroreduction, disk electrode rotation speed, diffusion kinetics*

https://doi.org/10.59849/0005-2531.2026.3.5

Introduction

Currently, thin-film functional materials form the basis of microelectronics, solar energy, sensors, nanotechnology, and photonics fields [1-8]. Such functional materials represent a rapidly developing area of materials science, aimed at creating substances with specified physical, chemical, or biological properties [9-16].

Antimony-based functional materials (Sb_2Te_3, GaSb, Sb_2Se_3, InSb, Sb_2S_3, etc.) are a broad group of substances in which antimony plays a key role in the formation of electrical, optical, thermoelectric, or catalytic properties. Such materials are actively used in electronics, optoelectronics, sensors, and energy [17-28]. Their properties are determined by the electronic structure, narrow band gap (Eg = 0.17–1.2 eV), high mobility of charge carriers, and anisotropy of the crystal lattice. They also have a high optical absorption capacity, sensitivity in the infrared range, and a higher refractive index [29-33].

The study of the electrodeposition or electroreduction process of the studied components is very important for their co-deposition [34-38]. With the help of this, the mechanism and area of potentials of their deposition are determined. From this point of view, electroreduction of antimony (Sb) has not only practical, but also fundamental importance. This process is a convenient model system for

studying electron transfer, forms of hydration of ions, surface phenomena on electrodes, and mechanisms of complexation. Along with this, research aimed at obtaining nanostructured antimony by electrochemical methods, as well as studying thermoelectric and photovoltaic properties of thin films based on it, is actively developing [39, 40].

In the analyzed literature, there are a number of works devoted to the electroreduction and deposition of antimony ions [40, 41].

The electrochemical behavior of antimony was elucidated by the preparation of antimony (Sb) particles in the deep eutectic solvent choline chloride ethylene glycol (ChCl-EG DES) at 333 K [41]. Cyclic voltammetry shows that the reduction of Sb(III) to Sb on the Ti electrode is a quasi-reversible process, and the diffusion coefficient D of Sb(III) remains in the range of 1.822×10^{-7} to 5.938×10^{-7} $cm^2 \cdot s^{-1}$ at 333 K. The effect of $SbCl_3$ concentration (10–100 mM) on cathodic and anodic polarization processes is discussed using linear sweep voltammetry. The initial nucleation of Sb on the titanium electrode is in good agreement with the three-dimensional nucleation process at 50–100 mM. Furthermore, cauliflower-shaped Sb particles with sizes of 1–1.2 μm can be deposited on a titanium substrate at various applied potentials (from −0.525 V to −0.675 V) and reaction times (10–600 s), formed by the aggregation of multiple spherical grains. Increasing the concentration of Sb(III) causes the formation of snowflake-shaped Sb particles [41, 42].

The work [35] is devoted to the study of the process of electrochemical deposition of antimony from a solution of antimony oxychloride in the presence of tartaric acid in an aqueous medium. Experimental results show that concentration, temperature, scanning speed, and the nature of the electrode influence the electroreduction of antimony ions from tartaric acid-based electrolytes. SEM, EDX, and X-ray diffraction data indicate that the Sb electrodepositions are characterized by high quality, purity, and strong adhesion to the substrate material. This confirms the presence of tartaric acid, which facilitates the electrodeposition process.

In [33], the authors show that, compared to an aqueous electrolyte in ethylene glycol, the electroreduction of antimony ions occurs at more negative potentials (-1.0 – (1.0) V). Here, the potential range of 0.4–0.01 V corresponds to the reaction $SbO^+ + e^- \rightarrow SbO$, 0.0 - (−0.43) V corresponds to the reaction $SbO + 2e^- \rightarrow Sb^{3+} + H_2O$, and -0.5 - (−0.87) V corresponds to the reaction $Sb^{3+} + 3e^- \rightarrow Sb^0$.

The authors of [43] studied the electrochemical reduction of Sb^{3+} in the H_2SO_4-NH_4F-SbF_3 electrolyte system. Linear scanning voltammetry measurements with different Sb^{3+} concentrations were recorded. The results show that the reduction of Sb^{3+} is a two-stage process, which is also confirmed by chronoamperometry, chronopotentiometry, and cyclic voltammetry data. In addition, the cyclic voltammetry results indicate that the reduction of Sb^{3+} is an irreversible diffusion-controlled process. The diffusion coefficients of Sb^{3+} in H_2SO_4-NH_4F-SbF_3 solution at different temperatures were calculated as 1.051×10^{-5} $cm^2 \cdot s^{-1}$ (298 K), 1.149×10^{-5} $cm^2 \cdot s^{-1}$ (303 K), 1.257×10^{-5} $cm^2 \cdot s^{-1}$ (308 K), 1.484×10^{-5} $cm^2 \cdot s^{-1}$ (313 K), and $2.120\times10^{-5} cm^2 \cdot s^{-1}$ (318 K), respectively. At various temperatures, the apparent activation energies of Sb^{3+} reduction at different overpotentials (from -0.23 V to -0.31 V) range from 16.932 kJ/mol to 14.647 kJ/mol. The low apparent activation energy also confirms that the Sb^{3+} reduction process is diffusion-controlled, as confirmed by cyclic voltammetry.

In this study [44], cyclic voltammetry (CV) and chronoamperometry (CA) tests were used to study the electrochemical behavior of antimony ions in KOH solution (20 wt%), and the results showed that Sb(III) ions have much higher electrochemical activity than Sb(V) ions. As reported in previous studies, Sb(V) ions cannot be considered completely inactive before the H_2 separation reaction, and a portion of Sb(V) ions can be electrodeposited in KOH solution. The discrepancies between current and previous studies originate from the additives

generated by Sb(III) ions, which are believed to play a role in the reduction of Sb(V) ions.

The authors of [45] show that the electroreduction of Sb^{3+} in ChCl-EG is a quasi-reversible reaction involving a diffusion-controlled, one-step, three-electron transfer process, which gives a diffusion coefficient D of 3.06×10^{-9} at 343 K. Temperature and concentration significantly affect the reduction of Sb(III) in ChCl-EG. Increasing the temperature and concentration decreases the overpotential required for Sb reduction. Current chromatographic studies show that at 343 K, Sb nucleation on the tungsten electrode occurs via a three-dimensional instantaneous nucleation. The applied deposition potential is the main driving force for the electroreduction of Sb(III). With the change in the applied deposition potential, the morphology of the antimony film gradually changes from granular to rod-shaped and then to dendritic.

To determine the redox processes in the presence of complexing agents, the electrochemical deposition of antimony (Sb) on gold in an HCl medium was investigated in [46]. Upon the addition of potassium antimony tartrate to the electrolyte, two reduction peaks were detected, corresponding to the reduction of SbO^+ and antimony tartrate, with the tartrate complex having a high reduction potential due to the high stability constant of the Sb-tartrate complex. The quasi-reversible electrochemical oxidation process reveals the significant role of the deposition type of Sb on Au. Adsorption studies of Sb particles on a gold electrode showed an increase in surface coverage with increasing adsorption time. The surface coverage of the Sb monolayer on gold after 5 min is estimated to be approximately 0.3, indicating irreversible deposition of Sb particles without potential bias. Thus, this study visualizes an irreversible deposition reaction dominated by ion adsorption and diffusion.

Analyzing the above studies, we can conclude that the electrochemical behavior of antimony ion reduction has been studied in various environments with varying kinetics. Therefore, the primary goal of our work is to determine the potential range and study the kinetics and mechanism of the electrochemical reduction of antimony ions in an acidic medium at pH 1.5. These studies are necessary for the further production of In-Sb thin films.

Experimental part

To prepare the electrolyte, antimony(III) oxide ("chemically pure" CAS: 1309-64-4, Sigma-Aldrich, Germany) was dissolved in a small amount of HCl. Then, 50 mL of bidistilled water was added, and the mixture was stirred. The electrolyte had the following composition: $(2\times10^{-4} – 1.4\times10^{-2})$ M $SbCl_3$.

Polarization curves were plotted using an IVIUMSTAT Electrochemical Interface potentiostat. A 100 ml glass three-electrode electrochemical cell was used. Pt with an area of 0.35 cm^2 and Ni with an area of 2 cm^2 were used as the working electrode, and a platinum plate with an area of 4 cm^2 was used as the auxiliary electrode. A silver chloride was utilized as the reference electrode.

A rotating disk electrode, brand RDE-710, Gamry Instruments, was used for kinetic studies. A glass three-electrode electrochemical cell with a volume of 100 ml was utilized. Here, Pt with an area of 0.2 cm^2 served as the working electrode, carbon as the auxiliary electrode, and a silver chloride electrode as the reference electrode.

Before the experiments, the surface of the Pt electrode was cleaned as follows: to oxidize and desorb many organic substances from the electrode surface, the Pt electrode was kept in concentrated H_2SO_4 for several minutes at a potential of 1.2 V. The electrode is maintained at a more negative potential of 0.0 V for reducing adsorbed oxygen. Next, the Pt electrode is maintained at a potential of 0.3 V for removing the adsorbed hydrogen, and thus its surface is completely cleaned [47].

Before experiments, the surface of the Ni electrodes is mechanically polished and dipped in diluted HNO_3 acid for 30 seconds to remove oxide layers, then immersed in alcohol or acetone, and finally washed with bidistilled water. Electrochemical polishing of the Ni

electrodes was carried out in a solution consisting of 55 ml H_2SO_4, 55 ml H_3PO_4, 50 ml H_2O (T = 293 - 303 K, i = 50 A / dm^2, τ = 180 sec), and then washed with bidistilled water [47].

The temperature of the electrolyte during the electrolysis process was maintained using a UTU-4 thermostat.

Results and discussion

Polarization curves were plotted to determine the potential range and study the kinetics and mechanism of the electrochemical reduction of antimony ions from an acidic electrolyte on various substrates—Pt, Ni, and Sb/Pt.

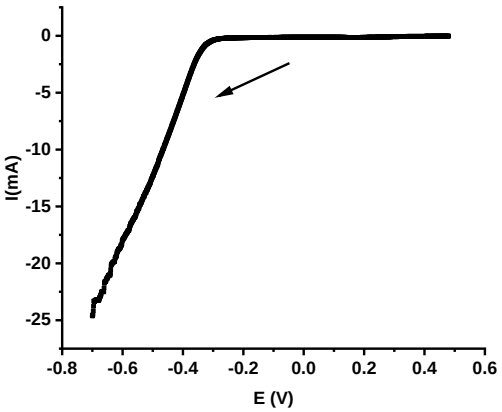

Fig. 1. Linear polarization curve of the background on the Pt electrode. pH=1.5.

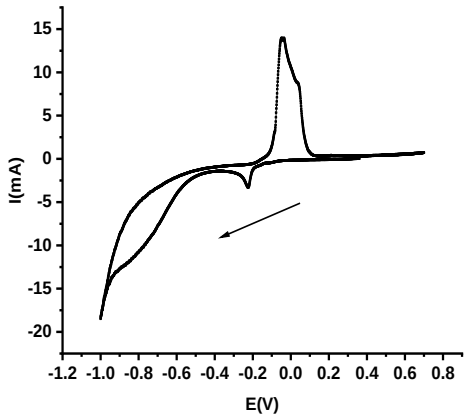

Fig. 2. Cyclic polarization curve of electroreduction of antimony ions from an acidic electrolyte on a Pt electrode. Electrolyte: 0.01 mol L^{-1} $SbCl_3$, pH = 1.5, T = 298 K, scanrate = 20 mV s^{-1}

Fig. 2 shows the cyclic polarization curve of the electroreduction of antimony ions from an aqueous electrolyte on Pt substrates. As can be seen from Fig. 2, in comparison with Fig. 1, in the initial stage, starting from -0.05 V potential, electroreduction of antimony ions occurs according to reaction (1):

$$SbCl_4^- + 3e^- = Sb + 4Cl^- \qquad (1)$$

After -0.35 due to the passivation of the electrode, the current spent on the process decreases. Furthermore, an increase in potential results in the current rising to 18 mA. The process, due to hydrogen separation, was studied down to -1.0 V potential. On the reverse polarization curve, the anodic dissolution of antimony ions is clearly observed in the potential range of -0.1 to 0.1 V.

Fig. 3 shows the cyclic polarization curve of the electroreduction of antimony ions from an aqueous electrolyte on Ni substrates. As can be seen from Fig. 3, starting from -0.2 to -0.35 V potential, the electroreduction of antimony ions occurs according to reaction (2) (peak a):

$$Sb^{3+} + 3e^- = Sb \qquad (2)$$

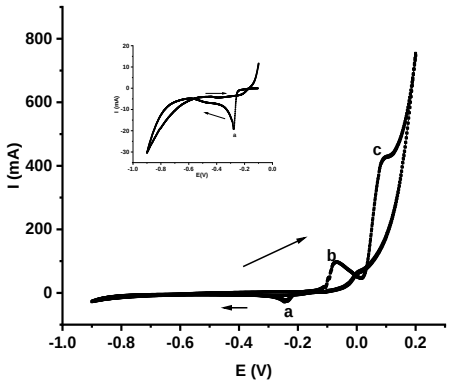

Fig. 3. Cyclic polarization curve of electroreduction of antimony ions from an acidic electrolyte on a Ni electrode. Electrolyte: 0.01 mol L^{-1} $SbCl_3$, pH = 1.5, T = 298 K, Scanrate = 20 mV s^{-1}

Subsequently, due to the passivation of the electrode, the current spent on the process decreases, and with an increase in potential, there is almost no further change in current.

This is due to the coating of the electrode surface with an antimony film. After -0.9 V, hydrogen separation is observed, and therefore, the process was studied up to this potential. On the anodic branch of the cyclic polarization curve, two clear peaks are visible. The first of them (peak b) refers to the reaction Sb^0-1e- = Sb^{1+}, and the second (peak c) corresponds to the reaction Sb^{1+}-2e- = Sb^{3+}.

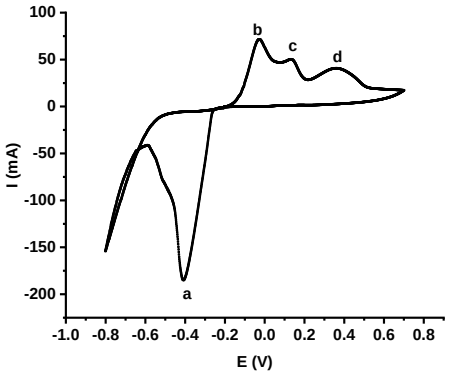

Fig. 4. Cyclic polarization curve of electroreduction of antimony ions from an aqueous electrolyte on a Sb/Pt electrode. Electrolyte: 0.01 mol L^{-1} $SbCl_3$, pH = 1.5, T = 298 K, Scanrate = 20 mV s^{-1}

The electroreduction of antimony ions from an aqueous electrolyte was also studied using a Sb/Pt electrode (Fig. 4). On the cathode branch of the polarization curve at the potential interval of -0.15 – (-0.56) V, the peak (a) is clearly visible, which corresponds to reaction (2). After -0.42 due to the passivation of the electrode, the current spent on the process decreases to 50 mA. We assume passivation occurs due to the simultaneous reduction of hydrogen ions with antimony ions, resulting in the formation of antimony hydride. Furthermore, after -0.56 V, a current increase to 155 mA is observed with increasing cathodic potential. After -0.8 V, hydrogen separation is observed, and therefore, the process was studied up to this potential. On the reverse path, that is, the anodic branch of the polarization curve, 3 peaks of anodic dissolution are clearly visible. Here, peak b corresponds to the reaction Sb^0-1e- = Sb^{1+}, peak c corresponds to the reaction Sb^{1+}-1e$^-$ = Sb^{2+}, and peak d corresponds to the reaction Sb^{2+}-1e$^-$ = Sb^{3+}.

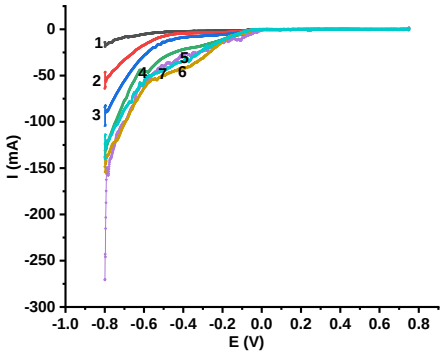

Fig. 5. Cathode polarization curves of antimony reduction on a rotating platinum electrode. Electrolyte composition (M): 0.01 mol L^{-1} $SbCl_3$; pH=1.5, scanrate= 20 mVs^{-1}, T=298 K. Electrode rotation speed: 1- 0; 2- 400; 3- 1600; 4- 3200 and 5- 4500; 6- 6400 and 7- 7200 rpm.

To elucidate the kinetics of the process during the electroreduction of antimony ions and obtain additional information on the nature of polarization, the rotating disk electrode (Pt) method was used. As can be seen from Fig. 5, increasing the rotation intensity significantly affects the speed of the cathodic process.

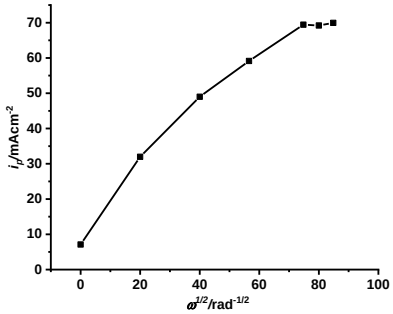

Fig. 6. Dependence of ip on the electrode rotation speed to the power of 0.5

Based on Fig. 5, a graph was plotted showing the dependence of the peak current on the rotation speed of the platinum disk electrode raised to the power of 0.5. This dependence (Fig. 6) for the process of antimony reduction is linear, and its slope is characteristic of diffusion processes [48].

Based on Fig. 5, the dependence of current density on the rotation speed of the disk electrode at various potentials was shown. As can be seen from Fig. 7, increasing the intensity of mixing at cathode potentials from -0.25 V to -0.26 V has little effect on the rate of the cathode process. The weak effect of stirring on the rate of the process indicates that at potentials up to −0.6 V, the limiting stage of the process is the transfer of active particles to the cathode surface; this indicates that diffusion polarization occurs. In addition, in all potentials studied, the value increases slightly with a mixing interval of 20–40 (rpm $^{-1}$)$^{1/2}$. This is due to the formation of a double electrical layer. After 40 (rpm^{-1})½, the diffusion rate increases, and antimony ions are more frequently deposited on the electrode surface.

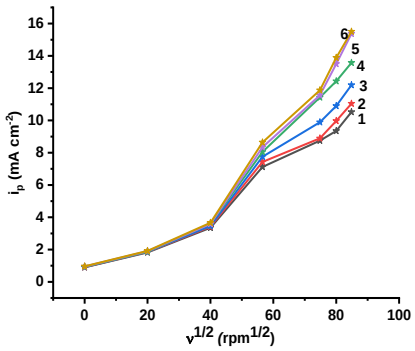

Fig. 7. Dependence of the peak current density on the rotation speed of the disk electrode. Electrolyte composition 0.01 mol L^{-1} $SbCl_3$; at potentials (V): 1 – (-0.25); 2 – (-0.26); 3 – (-0.27); 4 – (-0.28); 5 – (-0.29); 6 – (-0.3);

If we project these lines onto the vertical axis, we can see that at cathode potentials from -0.2 V to -0.3 V, all the lines intersect the axis near zero or up to 40 (rpm)$^{1/2}$, which is typical for processes where the limiting stage is the electrochemical kinetics of the deposited ions at the cathode surface. Additionally, after reaching 40 (rpm^{-1})½ and higher, the reaction rate with an increase in the electrode rotation speed increases, which indicates that at high rotation speeds of the disk electrode, the reaction rate of antimony reduction is determined by the diffusion kinetics (Fig. 7) [40].

To find the optimal electrolysis mode and electrolyte composition for the process of electroreduction of antimony ions, the influence of several different factors on the process was studied.

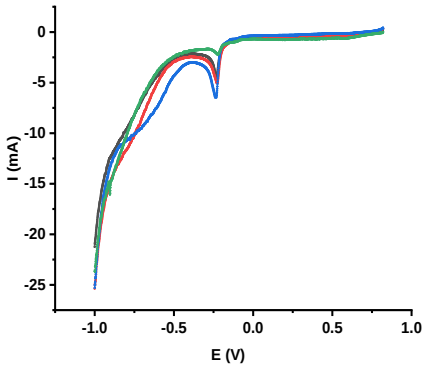

Fig. 8. Effect of antimony ion concentration on the process of electroreduction on Pt substrates. Electrolyte (mol/l): E_V = 0.02 V/sec., T=298K, $SbCl_3$ concentration (mol/l): green - 2×10^{-4}; black - 6×10^{-3}; 3 red - 0.01; blue - 0.014;

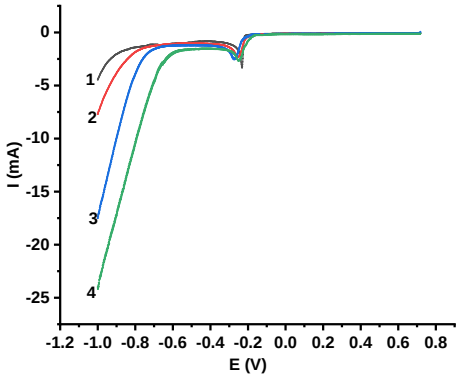

Fig. 9. Effect of temperature on the process of electroreduction on Pt substrates. Electrolyte (mol/L): 0.01 mol L^{-1} $SbCl_3$, E_V = 0.02 V/sec., T (°C): 1 - 298; 2 - 308; 3 - 318; 4 - 328;

Fig. 8 shows the linear polarization curves of the influence of antimony ion concentrations on the process of antimony electroreduction.

From the cathodic polarization curves, it is evident that increasing the concentration of antimony ions in the electrolyte has little effect on the process. In this case, the reduction potential will shift more towards the cathode.

The influence of temperature on the

process of electroreduction of antimony ions was also studied. The results are shown in Fig. 9. From the cathodic polarization curves, it is evident that with increasing temperature, the rate of electroreduction of antimony ions increases consistently. This is also confirmed by the increase in current on the polarization curves. Since at 298 K the current consumed in the process is 4.5 mA, and at 328 K – 24 mA. At this reduction potential, a shift towards a more cathodic region is observed.

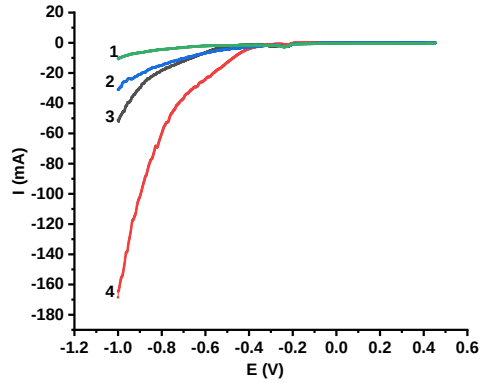

Fig. 10. Effect of scan rate on the process of electroreduction of antimony ions on Pt substrates. Electrolyte (mol/L): 0.01 mol L^{-1} $SbCl_3$. T=298K, Potential scan (V/sec): 1 - 0.005; 2 - 0.02; 3 - 0.04; 5 – 0.1.

The effect of the scan rate on the electroreduction of antimony ions was studied in the range of 0.005–0.1 V/sec. The linear polarization curves of the process are shown in Figure 10. As can be seen from the figure, with an increase in the scan rate, an increase in the current spent on the process of electroreduction of antimony ions from 15 mA to 170 mA is naturally observed.

Conclusion

The electrochemical reduction process of antimony ions at Pt, Ni, and Sb/Pt electrodes from an aqueous electrolyte was studied by plotting polarization curves. When studying the kinetics and mechanism of the process on a rotating disk electrode, it was determined that the electroreduction process is accompanied by diffusion kinetics. By graphically presenting the dependence of current density on the rotation speed of the disk electrode at various potentials, it was concluded that increasing the rotation speed of the electrode leads to an increase in the reaction rate. This indicates that, at high rotation speeds of the disk electrode, the rate of antimony reduction is determined by diffusion kinetics.

The results of all the experiments show that the process of electroreduction of antimony ions from an aqueous electrolyte is affected by temperature. As a result of studying the influence of these factors, the optimal electrolysis mode and electrolyte composition for the electrodeposition of antimony ions were selected.

References

1. Kaminski E., Suleymanov N., Minkovich B. et al. Waveguide Integrated Self-Powered MoS_2 Photodetectors in the Shortwave Infrared Wavelengths. *ACS Photonics*. 2025. V. 12. № 11. P. 6397–6405. https://doi.org/10.1021/acsphotonics.5c01893
2. Majidzade V.A., Mammadova S.P., Petkucheva E.S. et al. Co-electrodeposition of iron and sulfur in aqueous and non-aqueous electrolytes. *Bulgar. Chem. Commun*. 2020. V. 52. Special Issue E. P. 73-78
3. Singh B., Kumar R., Chandra B.G. et al. Enhancement of sunlight-driven water splitting via $TaSe_2$-functionalized Bi_2Se_3 and ZnSe photoelectrodes. *Mater. Chem. Phys*. 2026. V. 348. № 2. P. 131680. doi.org/10.1016/j.matchemphys.2025.131680
4. Javadova S.P., Majidzade V.A., Aliyev A.Sh., Tagiyev D.B. Effect of major factors on the composition of thin Bi_2Se_3 films. *Russ. J. Appl. Chem.* 2021. V. 94. № 1. P. 38-42
5. Gao S., He Y., Zhu K. et al. Heterointerface engineering-driven FeS_2/MoS_2 hollow porous nanofibers enable high-rate and ultra-long cycle sodium-ion batteries. *Chem. Eng. J.* 2025. V. 523. 168326. https://doi.org/10.1016/j.cej.2025.168326
6. Majidzade V.A., Aliyev A.Sh. Electrodeposition of $Ni_3Bi_2Se_2$ thin semiconductor films. *Iran. J. Chem. Chem. Eng.* 2021. V. 40. № 4. P. 1023-1029. https://doi.org/10.30492/ijcce.2020.43334
7. Liu L., Zhao W., Gao T. et al. $CoSe_2$/$MoSe_2$ heterojunction as an efficient electrocatalyst for energy-saving hydrogen production and electro-treatment of organic molecules. *Mater. Today Chem.* 2025. V. 48. 103000. https://doi.org/10.1016/j.mtchem.2025.103000

8. Sydorenko J., Krunks M., Katerski A. et al. Development of spray pyrolysis-synthesised Bi_2O_3 thin films for photocatalytic applications. *RSC Adv.* 2024. V. 14. P. 19648-19657. https://doi.org/10.1039/D4RA02907K
9. Javadova S.P., Majidzade V.A., Aliyev A.Sh. et al. Electrodeposition of Bi-Se thin films involving ethylene glycol-based electrolytes. *Electrochem. Sci. Eng.* 2021. V. 11. № 1. P. 51-58. https://doi.org/10.5599/jese.914
10. Hong W.T., Han M., Li Y. et al. Cobalt-Doped Magnetite Overlayer on Mo-Doped $BiVO_4$ Photoanode for Efficient Photoelectrochemical Water Oxidation. *ACS Mater. Lett.* 2024. V. 6. № 9. P. 4168-4174. https://doi.org/10.1021/acsmaterialslett.4c01151
11. Jafarova S.F., Majidzade V.A., Kasimogli I. et al. Electrical and Photoelectrochemical Properties of Thin MoS_2 Films Produced by Electrodeposition. *Inorg. Mater.* 2021. V. 57. № 4. P. 331–336. https://doi.org/10.1134/S0020168521040105
12. Abdullayev N.M., Ibrahimova L.N., Aliyev M.E., Aliyev Y.I. Investigation of the atomic dynamics of CdSe thin layers by Raman spectroscopy. *Chem. Prob.* 2024. V. 22. № 2. P. 231-236. https://doi.org/10.32737/2221-8688-2024-2-231-236
13. Babanly M.B., Mashadiyeva L.F., Imamaliyeva S.Z. et al. Thermodynamic properties of complex copper chalcogenides – review. *Chem. Prob.* 2024. V. 22. № 3. P. 243-280. https://doi.org/10.32737/2221-8688-2024-3-243-280
14. Wang Y., Huang Sh., Liu H. et al. Interlayer Electronic Hybridization for Friction Control in $MoSe_2/WS_2$ Heterostructures. *Nano-Micro Small.* 2025. V. 21. № 40. e06746. https://doi.org/10.1002/smll.202506746
15. Eminov Sh.O., Tagiyev D.B., Aliyev A.Sh. et al. Integration of supercapacitor with solar cell based on NiO_2 and CdS nanopillars embedded in porous anodic alumina templates. *Int. J. Energy Res.* 2022. V. 46. P. 22134-22144. https://doi.org/10.1002/er.8741
16. Abdullayeva S.H., Eminov Sh.O., Jalilova Kh.D. et al. Synthesis of anodic TiO2 nanotubes on Indium Tin Oxide-coated glass electrodes. *Int. J. Energy Res.* 2022. V. 46. P. 21686-21693. https://doi.org/10.1002/er.8667
17. Majidzade V.A., Jafarova S.F., Javadova S.P. et al. The latest progress on the synthesis and investigation of Sb_2S_3-based thin films. *Chem. Prob.* 2023. V. 21. № 2. P. 99-122. https://doi.org/10.32737/2221-8688-2023-2-99-122
18. Yu F., Wu Z., Qian Ch. et al. In-situ sulfur passivation enabling high open-circuit voltage in hydrothermally Sb_2S_3 solar cells. *Mater. Today Energy.* 2025. V. 54. 102083. https://doi.org/10.1016/j.mtener.2025.102083
19. Majidzade V.A., Aliyev A.Sh., Qasimogli İ. et al. Electrical properties of electrochemically grown thin Sb_2Se_3 semiconductor films. *Inorg. Mater.* 2019. V. 55. № 10. P. 979–983. https://doi.org/10.1134/S0020168519100108
20. Majidzade V.A., Aliyev A.Sh., Guliyev P.H., Babanly D.M. Electrodeposition of the Sb_2Se_3 thin films on various substrates from the Tartaric electrolyte. *Electrochem. Sci. Eng.* 2020. V. 10. № 1. P. 1-9. https://doi.org/10.5599/jese.676
21. Christianson A.M., Gabbaï F.P. *Antimony- and Bismuth-Based Materials and Applications.* Chapter 16 Main Group Strategies towards Functional Hybrid Materials. Book Editor(s): Thomas Baumgartner. Frieder Jäkle. 2017. https://doi.org/10.1002/9781119235941.ch16
22. Cheng L., Quan J., Li H. Recent advances in antimony-based anode materials for potassium-ion batteries: Material selection, structural design, and storage mechanisms. *Chinese Chem. Letters.* 2025. V. 36, № 9. 110685. https://doi.org/10.1016/j.cclet.2024.110685
23. Sutton M., Robertson N., Ameri T. Establishing design principles for functional additives in antimony chalcogenide solar cells. *J. Mater. Chem. A.* 2025. V. 13. P. 17340-17349. https://doi.org/10.1039/D5TA00947B
24. Mei J., Liu M., Vivo P., Pecunia V. Two-Dimensional Antimony-Based Perovskite-Inspired Materials for High-Performance Self-Powered Photodetectors. *Adv. Funct. Mater.* 2021. V. 31. № 50. 2106295. https://doi.org/10.1002/adfm.202106295
25. Fredj D., Alkarsifi R., Pourcin F. et al. A new antimony-based organic-inorganic hybrid material as electron extraction layer for efficient and stable polymer solar cells. *ACS Appl. Mater. & Interfaces.* 2019. V. 47. № 11. P. 44820-44828. https://doi.org/10.1021/acsami.9b12409
26. Murugesan S., Volokh M., Mokari T. Antimony-based materials for supercapacitor applications: A focused review. *J. Power Sources.* 2026. V. 669. 239338. https://doi.org/10.1016/j.jpowsour.2026.239338
27. Wang X., Su Sh., Fang D. et al. Facile synthesis and formation mechanism of uniform antimony nanotubes. *Funct. Mater. Lett.* 2017. V. 10. № 5. 1750064. doi.org/10.1142/S1793604717500643
28. Wang W., Hübner U., Gärtner A. et al. Three-dimensional Antimony Sulfide-Based Flat Optics. *Adv. Funct. Mater.* 2026. E 19065. https://doi.org/10.1002/adfm.202519065
29. Khelifi W., Capiod P., Barbot C. et al. Selective area molecular beam epitaxy of InSb on $InP(111)_B$: from thin films to quantum nanostructures. *Nanotechnology.* 2025. V. 36, № 12. 125301. https://doi.org/1088/1361-6528/adaafb.

30. Majidzade V.A., Aliyev G.S., Aliyev A.Sh. et al. Mathematical modeling and optimization of the electrodeposition process of the antimony-selenium system. *Azerb. Chem. J.* 2021. № 1. P. 30-36
31. Van T.N., Laborde E., Champeaux C. et al. Tunability of optical properties of InSb films developed by pulsed laser deposition. *Appl. Surf. Sci.* 2023. V. 619. 156756. https://doi.org/10.1016/j.apsusc.2023.156756
32. Majidzade V.A., Aliyev A.Sh., Tağıyev D.B. Electrochemical deposition of Sb_2Se_3 thin films semiconductor from tartaric acid solution. *Bulg. Chem. Commun.* 2020. V. 52. Special Issue E. P. 62-67
33. Majidzade V.A., Javadova S.P., Aliyev G.S. et al. Electrodeposition of Sb–Se Thin Films from Organic Electrolyte. *Chem. Afr.* 2022. V. 5. № 6. P. 2085-2094. https://doi.org/10.1007/s42250-022-00480-8
34. Majidzade V.A., Aliyev A.Sh., Babanly D.M. et al. Investigation of the electrochemical reduction process of the molybdate ions in the tartaric electrolytes. *Acta Chim. Slov*. 2019. V. 66. № 1. P. 155-162. https://doi.org/10.17344/acsi.2018.4733
35. Majidzade V.A., Guliyev P.H., Aliyev A.Sh. et al. Electrochemical characterization and electrode kinetics for antimony electrodeposition from its oxychloride solution in the presence of tartaric acid. *J. Mol. Struc.* 2017. V. 1136. P. 7-13. https://doi.org/10.1016/j.molstruc.2017.01.082
36. Javadova S.P., Majidzade V.A., Jafarova S.F. et al. Electrochemical behavior of bismuth ions in citrate solutions. *Azerb. Chem. J*. 2023. № 4. P. 5-12. https://doi.org/10.32737/0005-2531-2023-4-5-12
37. Majidzade V.A., Aliyev A.Sh., Elrouby M. et al. Electrodeposition and Growth of Iron from an Ethylene Glycol Solution. *Acta Chim. Slov*. 2021. V. 68. № 1. P. 185-192. https://doi.org/10.17344/ACSI.2020.6308
38. Majidzade V.A. Electroreduction of thiosulphate ions from non-aqueous solutions. *Azerb. Chem. J.* 2020. № 2. P. 61-66. https://doi.org/10.32737/0005-2531-2020-2-61-66
39. Zhou Y., Wang L., Chen Sh. et al. Thin-film Sb_2Se_3 photovoltaics with oriented one-dimensional ribbons and benign grain boundaries. *Nat. Photon.* 2015. V. 9. № 6. P. 409-415. doi.org/10.1038/nphoton.2015.78
40. Toberer E.S., Zevalkink A., Jeffrey Snyder G. Phonon engineering through crystal chemistry. *J. Mater. Chem*. 2011. V. 21. № 40. P. 15843-15852. https://doi.org/10.1039/C1JM11754H
41. Bu J., Ru J., Hua Y. et al. Electrochemical behavior of Sb(III)/Sb during the preparation of Sb particles in deep eutectic solvent. *Ionics*. 2021. V. 27. P. 3119–3127. https://doi.org/10.1007/s11581-021-04048-3
42. Bu J., Ru J., Wang Zh. et al. Controllable preparation of antimony powders by electrodeposition in choline chloride–ethylene glycol. *Adv. Powder Technol.* 2019. V. 30. № 12. P. 2859-2867. https://doi.org/10.1016/j.apt.2019.06.027
43. Lin Y., Ning P., Cui Y. et al. Electrodeposition Behaviour of Antimony in H_2SO_4-NH_4F-SbF_3 Solutions. *Int. J. Electrochem. Sci.* 2019. V. 14. P. 4003 – 4019. https://doi.org/10.20964/2019.03.33
44. Wang Q., Wang Y. Fundamental Electrochemical Behavior of Antimony in Alkaline Solution. *J. Sustain. Metall.* 2019, V. 5. P. 606–616. https://doi.org/10.1007/s40831-019-00253-7
45. Wang H., Cao X.Z., Xue X.X. Study on electrodeposition of antimony in choline chloride-ethyleneglycol eutectic solvent. *J. Electrochem.* 2022. V. 28. № 4. 2103071. https://doi.org/10.13208/j.electrochem.210307
46. Antony R.P., Sasi S.K., Subramanian H. et al. Role of tartarate ion in antimony deposition on gold in acidic medium. *AIP Conf. Proc*. 2020. V. 2265. 030306. https://doi.org/10.1063/5.0016680
47. Barkovskij V.F., Gorodenceva T.B., Toporova N.B. Osnovy fiziko-himicheskih metodov analiza. M: Vysshaya shkola, 1983. 247 s. (in Russian)
48. Pleskov Yu.V., Filippovskiy V.Yu. *Vrashchayushchiysya diskovyy elektrod*. Nauka Publ. Moscow. Russia. 1972. 344 s. (In Russian)

TURŞ ELEKTROLİTDƏN SÜRMƏ İONLARININ ELEKTROREDUKSİYA PROSESİNİN ÖYRƏNİLMƏSİ

N.A. Əliyeva Məmmədova, S.F. Cəfərova, S.P. Cavadova, Ş.A. İbrahimova, A.A. Əliyev, S.D. Dadaşova, M.F. Nəbiyeva, M.T.Abbasov, H.Ç. Əliyeva, D.B. Tağıyev

Tədqiqat işində turş elektrolitdən sürmə ionlarının elektroreduksiya prosesi öyrənilmişdir. Tsiklik polyarizasiya əyrilərinin çəkilməsi ilə müxtəlif elektrodlarda sürmə ionlarının elektroreduksiya potensial oblastı müəyyən edilmişdir. Sürmə ionlarının elektroreduksiya prosesinə bir neçə amilin təsiri də öyrənilmişdir. Müəyyən edilmişdir ki, temperaturun artması sürmə ionlarının elektroreduksiya sürətini artırır. Bundan əlavə, polyarizasiya əyriləri fırlanan platin disk elektrodu istifadə edilərək çəkilmişdir. Əldə edilən məlumatlar, yəni i_p-in elektrodun fırlanma sürətindən (ω) xətti asılılığı, sürmə ionlarının elektroreduksiya prosesinin diffuzion kinetikası ilə müşayiət olunduğunu təsdiqləyir. Müxtəlif potensiallarda cərəyan sıxlığının elektrodun fırlanma sürətindən asılılığı da bu nəticəni təsdiq edir.

Açar sözlər: sürmə ionları, polyarizasiya, elektroreduksiya, fırlanan disk elektrodu, diffuzion kinetika